Quantifying Dispersion in Graphene Oxide/Reactive Benzoxazine Monomer Nanocomposites

ARTICLE *in* MACROMOLECULES · MAY 2014

Impact Factor: 5.8 · DOI: 10.1021/ma500334j

3 AUTHORS, INCLUDING:

Carlos Rodriguez Arza
Case Western Reserve University
10 PUBLICATIONS **84** CITATIONS
SEE PROFILE

Hatsuo Ishida
Case Western Reserve University
448 PUBLICATIONS **12,896** CITATIONS
SEE PROFILE

Macromolecules

Article

pubs.acs.org/Macromolecules

Quantifying Dispersion in Graphene Oxide/Reactive Benzoxazine Monomer Nanocomposites.

Carlos R. Arza,[†] Hatsuo Ishida,[‡] and Frans H. J. Maurer[†,*]

[†]Department of Chemistry, Polymer & Materials Chemistry, Lund University, Box 124, Lund, Sweden

[‡]Department of Macromolecular Science and Engineering, Case Western Reserve University, Cleveland, Ohio 44106-7202, United States

Supporting Information

ABSTRACT: Two structurally different bisbenzoxazine monomers (*t*BP-oda and *t*BP-jeff$_{148}$) are synthesized and reinforced with graphene oxide (GO) at concentrations ranging from 0.25 to 3 wt %. Successful synthesis of the benzoxazine monomer and conversion from graphite to GO are verified by proton nuclear magnetic resonance spectroscopy (^{1}H NMR), Fourier transform infrared spectroscopy (FT-IR), and X-ray diffraction (XRD), respectively. Dispersibility of GO in the benzoxazine monomers prior to polymerization is studied using rheological analysis, and quantified according to the theory of fractal model of colloidal gels. The polymerization behavior of the GO/benzoxazine mixtures is studied by both differential scanning calorimetry (DSC) and dynamic mechanical analysis (DMA). Rheological analysis is also applied to the nanocomposite precursors. Better dispersions are achieved using *t*BP-oda, the benzoxazine with a high degree of aromaticity in its chemical structure. The addition of GO exhibits a negative effect on the polymerization of the two benzoxazines. The mechanical properties and the glass transition temperature T_g of GO/poly(*t*BP-oda) nanocomposites increases, whereas for the GO/poly(*t*BP-jeff$_{148}$) nanocomposites, the mechanical properties are moderately enhanced and T_g is reduced as a function of the GO concentration. The modifications of the mechanical and thermal properties of the nanocomposites are mainly attributed to the degree of dispersion of the GO nanosheets.

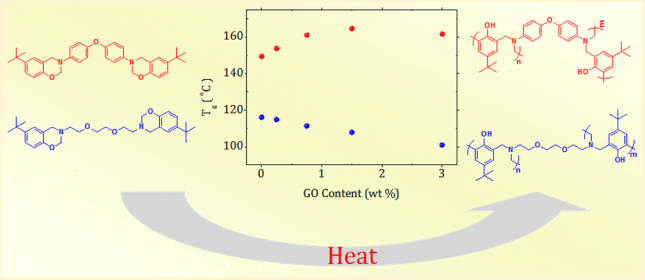

INTRODUCTION

Polybenzoxazines are a class of thermosets whose remarkable set of properties have attracted much attention in the last few decades.[1] Among such properties are near-zero shrinkage during polymerization, high thermal stability, flame retardancy, good mechanical strength, low dielectric constant, and good reactivity and compatibility with other polymers.[2−5] In addition, the molecular design flexibility with which the polybenzoxazine precursors can be prepared makes the tailoring of well-defined molecular structures for specific applications possible.[1] However, relatively high temperatures for the polymerization reaction of benzoxazines as well as low toughness, inherent to most thermosets, are considered as limitation for several applications. Through the preparation of a second group of polybenzoxazine precursors, where benzoxazine moieties are incorporated either in a flexible polymer main chain or as pendant groups, toughness and properties such as, ductility, and processability can be enhanced notably.[6−12] On the other hand, the addition of inorganic particles to polymers for the preparation of composites is also an important method to produce materials with increased stiffness, toughness, controlled mechanical damping, dimensional stability, and lower gas permeability, compared to those of the neat polymer.[13,14] Further improvements are achieved with the introduction of nanosize fillers to the polymer matrix where substantial changes in properties are obtained at very low loadings (<2 vol %).[15−20] Graphene oxide is an excellent precursor for the preparation of graphene,[21] and has been used to prepare polymer nanocomposites with remarkable results.[22−26] Graphene oxide (GO) is a single layer material obtained by oxidation of graphite[27−29] and subsequent exfoliation.[30] The main reasons for the use of graphene oxide as a reinforcing material are its very high aspect ratios (lateral size on the order of 1 μm and thickness between 0.7 and 1 nm),[26,31,32] a Youngs modulus as high as 200 GPa, and a versatile surface chemistry.[33] To achieve good material performance, however, not only the intrinsic properties of the filler are important, but also aspects such as interfacial chemistry and dispersibility. The latter playing a decisive role in the structure-properties relations.[13,34−40] In this study, two different benzoxazine monomers were synthesized and used as matrices for the preparation of graphene oxide nanocomposites. By varying the degree of aromaticity of the chemical structure as well as the hydrophilicity of the benzoxazines, the state of dispersion of graphene oxide is assessed by analyzing the rheological and dynamical mechanical properties of the nanocomposites.

Received: February 13, 2014
Revised: May 6, 2014
Published: May 21, 2014

   dx.doi.org/10.1021/ma500334j | *Macromolecules* 2014, 47, 3685−3692

EXPERIMENTAL SECTION

Materials. 4,4′-Oxydianiline (ODA) (97%), sulfuric acid (H_2SO_4) (96%), potassium permanganate ($KMnO_4$) (97%), and 1-butanol were purchased from Sigma-Aldrich. 4-*tert*-Butylphenol (*t*BP) (97%), sodium hydroxide (NaOH) (extra pure), and hydrogen peroxide (H_2O_2) (35% in water) were purchased from Acros Organics. Chlorobenzene (for synthesis), ortho-phosphoric acid (H_3PO_4) (85%), and methanol (HPLC grade) were purchased from Merck Millipore. Hexane (96%), and magnesium sulfate anhydrous ($MgSO_4$) (extra pure) were purchased at Scharlau. 2,2′-(Ethylenedioxy)bis-(ethylamine) (Jeffamine EDR-148) (Jeff148) (97%) was purchased from Huntsman. Paraformaldehyde (≥95%) was purchased from Fluka. Dimethylformamide (DMF) (HPLC grade) was purchased from Fisher Scientific. Graphite was kindly supplied by Asbury Graphite Mills (Expandable Graphite grade 3807). All chemicals were used as received.

Synthesis of Graphite Oxide. Graphite oxide was prepared according to the improved synthesis of graphite oxide.[41] Graphite (2 g) was added to a 9:1 mixture of H_2SO_4 (245 mL) and H_3PO_4 (27.2 mL) under mechanical stirring. In an ice bath, $KMnO_4$ (10 g) was added portion-wise for 10 min. The reaction mixture was then heated to 50 °C and stirred for 14 h. Once at room temperature, the reaction mixture was gradually poured into ice (450 mL) and H_2O_2 (ca. 5 mL). After 30 min, the golden mixture was centrifuged at 10000 rpm for 20 min, and the supernatant was discarded. By centrifugation, the sediment was washed successively with H_2O (500 mL), 10% HCl (500 mL), and methanol (500 mL) (repeating twice the succession), and finalizing with H_2O (500 mL × 4). Finally, the brown suspension was dried under vacuum at 50 °C for 48 h. (XRD patterns in Figure 1SI in the Supporting Information).

Synthesis of 3,3′-(4,4′-Oxybis(4,1-phenylene))bis(6-*tert*-butyl-3,4-dihydro-2*H*-benzo[*e*][1,3]oxazine) (*t*BP-oda). *t*BP (3.04 g, 20.26 mmol, 2 equiv) and ODA (2.03 g, 10.13 mmol) were dissolved in 24 mL of a 8:2 solvent mixture of chlorobenzene and toluene at 120 °C. In 2 mL of the same solvent mixture, paraformaldehyde (1.33 g, 44.57 mmol, 4.4 equiv) was suspended, and added to the solution portionwise for 5−7 min. After 4.5 h, the reaction mixture was dried under a stream of N_2 overnight. Finally, the resulting solid was washed three times with cold butanol, and dried under vacuum at 50 °C overnight to give an orange-like powder (yield: 80%). ^{1}H NMR (400 MHz, $CDCl_3$, 20 °C) δ, ppm; 7.20−6.74 (Ar), 5.30 (O−**CH_2**−N), 4.60 (Ar−**CH_2**−N), and 1.29 (−CH_3). FT-IR ν (cm^{-1}); 1498 (trisubstituted benzene ring), 1229 (oxazine C−O−C), 936 (out-of-plane C−H), and 817 (trisubstituted benzene ring) (Figure 2SIa, Supporting Information).

Synthesis of 6-*tert*-Butyl-3-((2-(2-(6-*tert*-butyl-2*H*-benzo[*e*]-[1,3]oxazin-3(4*H*)-yl)ethoxy)ethoxy)methyl)-3,4-dihydro-2*H*-benzo[*e*][1,3]oxazine (*t*BP-jeff$_{148}$). *t*BP (3.27g, 21.74 mmol, 2 equiv), Jeff148 (1.61 g, 10.87 mmol), and paraformaldehyde (1.43 g, 47.89 mmol, 4.4 equiv) were reacted during 3 h in 7 mL of a 8:2 solvent mixture of CB and toluene at 120 °C. The reaction mixure, was concentrated by stream of N_2 overnight. The resulting syrup was diluted in hexane, and washed 4 times with 0.2 N NaOH and 4 times with water. The organic phase was dried with anhydrous $MgSO_4$ and rotary evaporated (yield: 77%). ^{1}H NMR (400 MHz, $CDCl_3$, 20 °C) δ, ppm; 7.19−6.70 (Ar), 4.89 (O−**CH_2**−N), 4.06 (Ar−**CH_2**−**N**), 3.70 (N−CH_2−**CH_2**−O), 3.67 (O−**CH_2**−**CH_2**−O), 3.02 (N−**CH_2**−CH_2−O), and 1.29 (−CH_3). FT-IR ν (cm^{-1}); 1499 (trisubstituted benzene ring), 1229 (oxazine C−O−C), 933 (out-of-plane C−H), and 818 (trisubstituted benzene ring) (Figure 2SIb, Supporting Information).

Preparation of the GO/Benzoxazine Mixtures. Benzoxazine monomer (0.25 g) and a suitable amount of graphite oxide were added to 2 mL DMF, and shaken until the monomer was dissolved. The dispersions were obtained after exfoliation of graphite oxide into GO by means of ultrasonic irradiation (Branson Ultrasonic Cleaner model 2510E-MTH) for 20 min for the series prepared with *t*BP-oda, and 40 min for the series prepared with *t*BP-jeff$_{148}$. Finally, the dispersions were cast on porcelain crucibles at 70 °C for 16 h, and dried under vacuum at 50 °C for 48h.

Scheme 1. Synthesis of (a) *t*BP-oda and (b) *t*BP-jeff$_{148}$

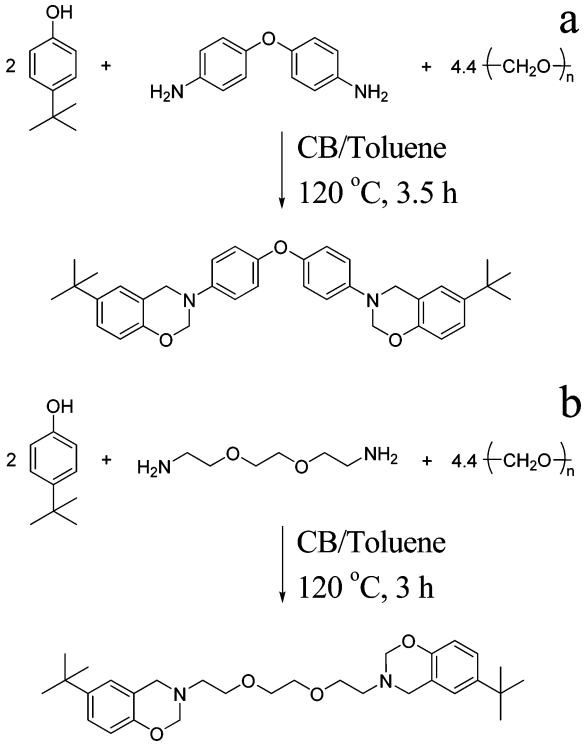

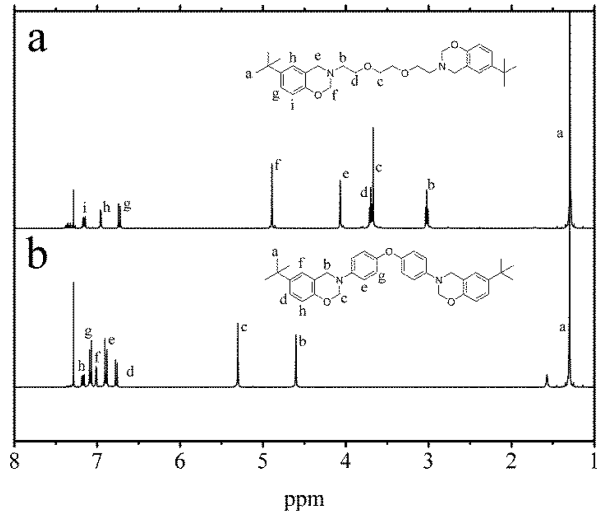

Figure 1. ^{1}H NMR spectra of (a) *t*BP-jeff$_{148}$, and (b) *t*BP-oda.

Characterization. ^{1}H NMR data was collected on a Bruker DRX400 spectrometer at the proton frequency of 400.13 MHz with $CHCl_3$-d_6 (δ = 7.26 ppm) used as an internal standard.

FT-IR-spectra were measured with an attenuated total reflection (ATR) setup using a Bruker Alpha FT-IR spectrometer. Twenty four scans were coadded using a resolution of 4 cm^{-1}.

XRD patterns were recorded with a Stoe Stadi MP Diffractometer in the reflection mode using Cu Kα radiation (0.15418 nm).

Differential scanning calorimetry (DSC) measurements were performed using TA Instruments DSC Q2000. The two series were studied with a heating rate of 10 °C/min under nitrogen with the purge rate of 60 mL/min. In addition, each series were studied simulating the conditions used in the rheometer for the study of the polymerization behavior of the nanocomposites. The samples prepared with *t*BP-oda were subjected to an isothermal stage at 140 °C for 30 min, cooled to 130 °C, heated to 225 °C at a rate of 3 °C/min, and finally maintained at 225 °C for 25 min. The samples prepared with

dx.doi.org/10.1021/ma500334j | *Macromolecules* 2014, 47, 3685−3692

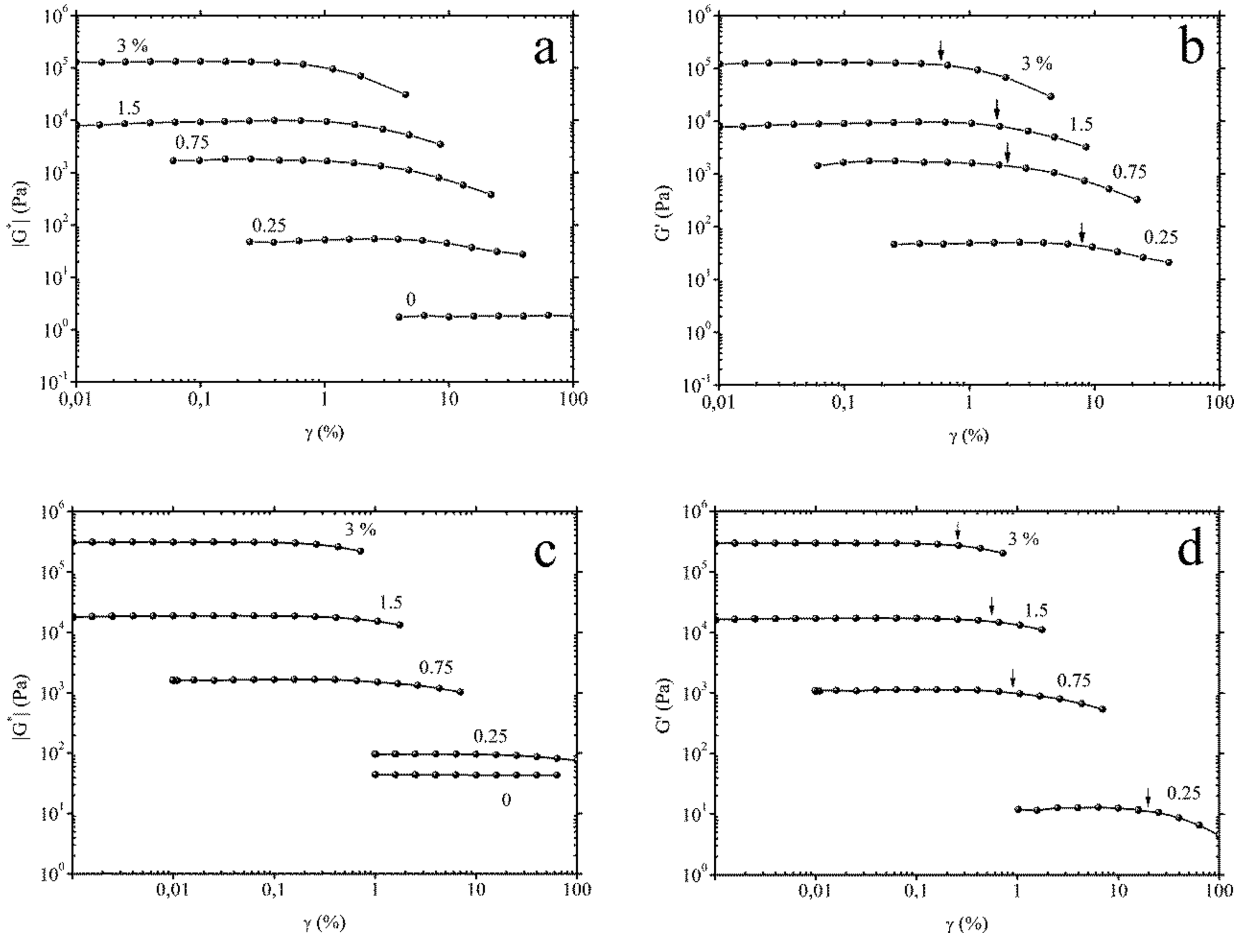

Figure 2. Dynamic shear modulus |*G**| and storage modulus *G*′ as a function of the strain amplitude at 6.28 rad/s for *t*BP-oda series at 140 °C (a and b) and *t*BP-jeff$_{148}$ series at 50 °C (c and d). Critical shear strains γ_c are indicated by the arrows.

*t*BP-jeff$_{148}$ were heated from 40 to 215 °C at a rate of 3 °C/min, and maintained at 215 °C for 25 min.

Dynamic mechanical analysis (DMA) was performed in an Advance Rheometer AR2000 ETC from TA Instruments. Rheological characterization was carried out under N_2 atmosphere, and using parallel plates with a diameter of 15 mm and a gap of ca. 1 mm, with the exception of samples of pure *t*BP-oda where a diameter of 25 mm was employed instead. *t*BP-jeff$_{148}$ series were studied at 50 °C, whereas *t*BP-oda series were studied at the melting temperature of the pure monomer at 140 °C (Figure 3SI, Supporting Information). After the samples were loaded, a time sweep at a small amplitude at 6.28 rad/s was performed until the dynamic shear modulus |*G**| remained unchanged (a few minutes). Afterward, strain sweeps at 6.28 rad/s were carried out and the critical strain γ_c was determined as the strain where the storage modulus *G*′ dropped to 90%. After waiting for a few minutes, a sufficient time to observe a constant |*G**| in a time sweep at an amplitude below γ_c, a frequency sweep at the aforementioned strain amplitude was carried out. The polymerization behavior of the GO/benzoxazines mixtures was studied by performing a temperature ramp at 3 °C/min followed by a time sweep of 25 min at 225 °C for samples prepared with *t*BP-oda, and at 215 °C for samples prepared with *t*BP-jeff$_{148}$, both series at 6.28 rad/s and at $\gamma < \gamma_c$. Finally, in a subsequent cooling temperature ramp at 3 °C/min, at 0.01% strain amplitude and at 6.28 rad/s, dynamic mechanical properties of the nanocomposites were studied.

RESULTS AND DISCUSSION

Two bisbenzoxazines with different chemical structure in the diamine component were prepared in order to compare the ability to disperse GO nanoplates, and to study the reinforcing effect on the final nanocomposites. The difference between the two monomers is found in the aromaticity and hydrophilicity in diamine components. Scheme 1 shows the two benzoxazine monomers for which the chemical structure was confirmed by NMR spectra, as shown in Figure 1.

Rheological measurements. To study the limits of the linear viscoelastic behavior of the GO/benzoxazine mixtures, strain sweeps were performed at 6.28 rad/s, at 50 °C for *t*BP-jeff$_{148}$ and 140 °C for *t*BP-oda series. The higher temperature employed of the latter series was to avoid crystallization of the benzoxazine monomer (Figure 3SI, Supporting Information). Figure 2 shows the dynamic shear modulus |*G**| and the storage modulus *G*′ of the two series as a function of the strain amplitude. Both systems displayed an enhancement of |*G**| and *G*′ as the amount of GO increased from 0.25 to 3 wt %. Additionally, the limit of linearity, characterized by the critical strain γ_c (as defined above), was observed to decrease with increasing concentration of GO nanosheets (Figures 2b and 2d). Such decrease of γ_c is expected to occur for percolating aggregated networks, which show a power-law dependency on the volume fraction ϕ of the aggregates.[42−46] Similar power-law dependency on the volume fraction of GO was observed in the systems used in this study which will be used later for further analysis.

Figure 3 shows dynamic frequency sweeps conducted at $\gamma < \gamma_c$ for the two series. Pure monomers show perfect Newtonian behavior as observed from the unity slope in the log frequency dependency of log |*G**|. The dynamic shear modulus |*G**| for

dx.doi.org/10.1021/ma500334j | *Macromolecules* 2014, 47, 3685−3692

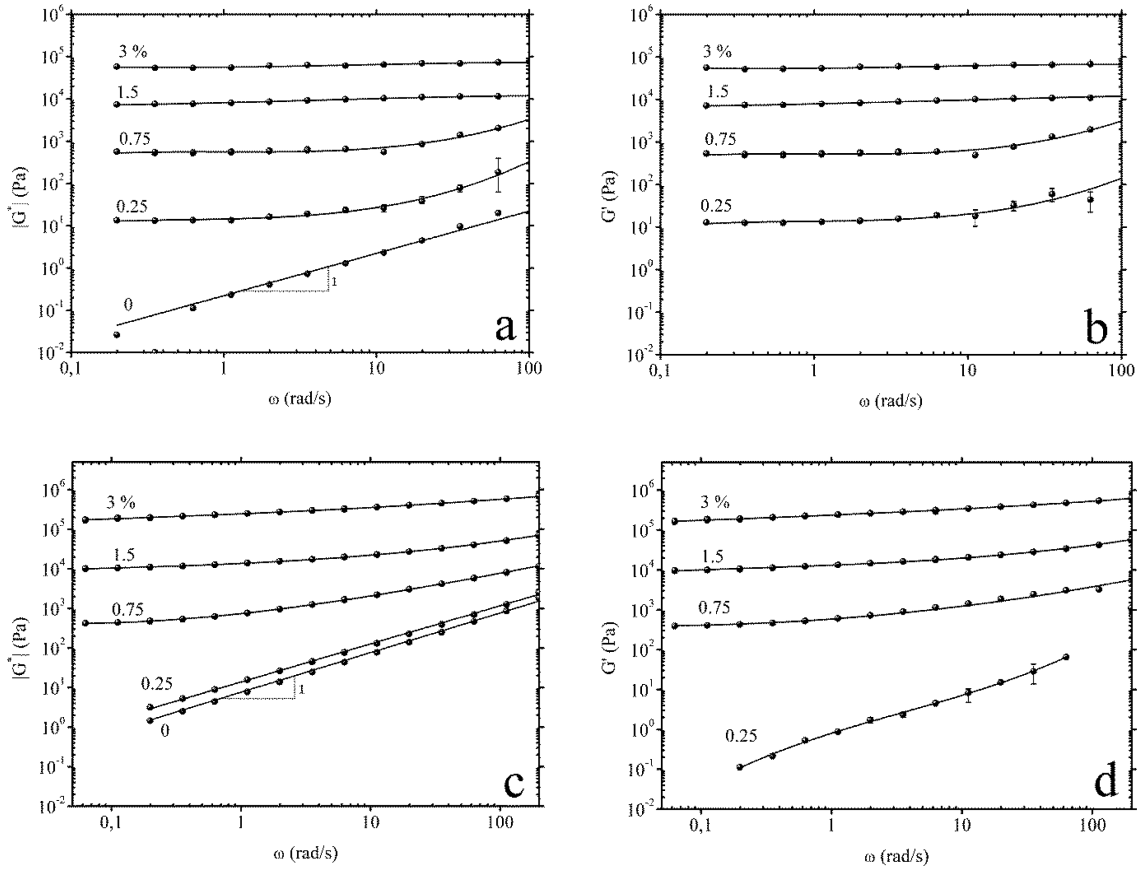

Figure 3. Dynamic shear modulus |G*| and storage modulus G' as a function of frequency for *t*BP-oda series at 140 °C (a and b) and *t*BP-jeff$_{148}$ series at 50 °C (c and d).

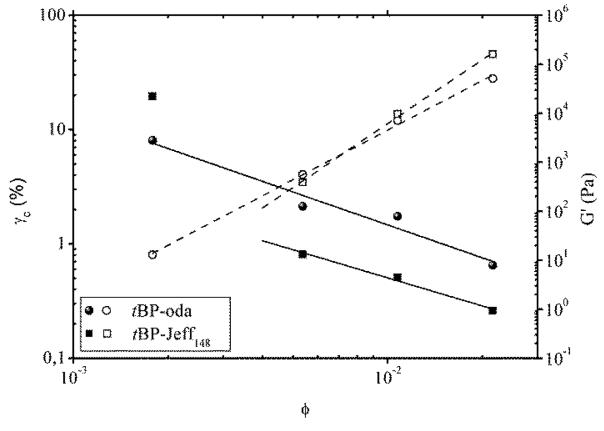

Figure 4. Critical strains at 6.28 rad/s for *t*BP-oda series at 140 °C (●) and *t*BP-jeff$_{148}$ series at 50 °C (■) as a function of volume fraction. Storage moduli at low frequencies for *t*BP-oda series at 140 °C (○) and *t*BP-jeff$_{148}$ series at 50 °C (□) as a function of volume fraction. Straight and dashed lines represent the regression fits.

both series increased with the concentration of GO for the entire range of frequency, where enhancements of approximately 6 decades in |G*| at 0.1 rad/d were observed for GO/Benzoxazine mixtures containing only 3 wt % GO. Furthermore, the storage modulus G' of the two series displayed a plateau at low frequency, at concentrations equal and higher than 0.25 wt % GO for GO/*t*BP-oda mixtures, whereas the plateau for the *t*BP-jeff$_{148}$ series was observed at concentrations equal and higher than 0.75 wt % GO. Such frequency-independent behavior of the elastic properties of a viscoelastic material stems from the formation of a space-filling elastic network, which in this study corresponds to a network formed by GO nanoplatelets. The percolation volume fraction for network formation ϕ_p for GO/*t*BP-oda mixtures would then lie below 0.25 wt % GO as opposed to a value between 0.25 and 0.75 wt % GO for the series prepared with *t*BP-jeff$_{148}$. The lower value for the percolation threshold of the *t*BP-oda series was attributed to a better dispersion of the GO nanoplatelets.[47] In line with these results, low rheological and electrical percolations have also been reported in the literature for graphene-based nanocomposites.[48−50]

According to the scaling theory of percolated colloidal gels based on fractal concepts, further analysis on the dispersion of GO was made. Shihet al.[45] proposed a series of relationship where both the elastic moduli and the limits of linearity of a colloidal gel scale the volume fraction of particles in a power-law fashion, assuming the links between the flocs being stronger than the links between the particles within the floc, according to

$$G' \propto \phi^{(3+b)/(3-D)} \tag{1}$$

$$\gamma_c \propto \phi^{-(1+b)/(3-D)} \tag{2}$$

where D is the fractal dimension of the aggregates and b is the fractal dimension of the backbone of the aggregate. Figure 4 shows G' at 0.2 rad/s for GO/*t*BP-oda mixtures and at 0.063 rad/s for GO/*t*BP-jeff$_{148}$ mixtures together with the critical strains γ_c as a function of GO volume fraction for the two series. As observed, similar power-law scaling of γ_c on ϕ were

dx.doi.org/10.1021/ma500334j | *Macromolecules* 2014, 47, 3685−3692

obtained for both series: $\gamma_c \propto \phi^{-0.96}$ for *t*BP-oda series and $\gamma_c \propto \phi^{-0.82}$ for *t*BP-jeff$_{148}$ series. It is worth mentioning that despite the existence of a critical strain for samples containing 0.25 wt % GO from the *t*BP-jeff$_{148}$ series, it did not appear as a consequence of the disruption of the GO network. Instead, it was the alignment of the dispersed nanoplatelets with the shear force direction due to hydrodynamic forces that caused the reduction of the contribution to the dynamic shear modulus. The power-law scaling of G' on ϕ was determined to be $G' \propto \phi^{3.36}$, and $G' \propto \phi^{4.33}$ for GO/*t*BP-oda and GO/*t*BP-jeff$_{148}$ mixtures, respectively. The higher value of the power-law exponent suggests the higher efficiency in storing elastic energy for the GO network formed in the *t*BP-jeff$_{148}$ series than in the *t*BP-oda series. Solving eqs 1 and 2 gives $D = 2.17$ for the *t*BP-oda series and $D = 2.43$ for the *t*BP-jeff$_{148}$ series. Lower values for the fractal dimension D suggests a more open fractal structure and therefore a better exfoliation of the GO nanoplatelets in the *t*BP-oda samples,[40] which is in agreement with the finding of a lower percolation volume fraction for this series. However, the obtained values for the fractal dimension of the backbone of the aggregates were $x = -0.20$ and $x = -0.54$ for the *t*BP-oda and *t*BP-jeff$_{148}$ samples, respectively, which lie outside the boundary condition of $1 < x < D$ in order for the theory to apply. This indicates the existence of local aggregate structures in the GO network that were not fractal and that it is thus complicated to relate x to the degree of exfoliation. Vermant et al. found similar results for montmorillonite-reinforced polypropylene.[40]

Analysis of the Polymerization Process by DMA. Figure 5 shows the evolution of the dynamic shear modulus $|G^*|$ for the two series. *t*BP-oda series were studied at 140 °C as starting temperature due to crystallization of the benzoxazine monomer. The dynamic shear modulus $|G^*|$ of pure *t*BP-oda remained practically unchanged during the temperature ramp until the ring-opening reaction of the oxazine became effective, provoking a rapid increase of about five decades due to linear polymerization and further cross-linking. A final isothermal treatment at 225 °C was programmed during 25 min to complete the polymerization of the benzoxazine. Longer time resulted in slight structural rearrangements as observed by the decrease of the dynamic shear modulus.[1] The polymerization behavior of the GO/*t*BP-oda mixtures showed a similar behavior to that of the pure benzoxazine, with the difference of the initial shear modulus being dramatically enhanced with the addition up to 3 wt % of the GO nanoplatelets. Additionally, a reduction of the onset of the polymerization with the concentration of GO is observed, as well as a consistent increase of the mechanical properties of the nanocomposites at 225 °C up to almost one decade for samples containing 3 wt % GO. For the *t*BP-jeff$_{148}$ series, a drop on the dynamic shear modulus $|G^*|$ was observed during the first minutes of the temperature ramp attributed to the softening of the material as temperature increased. From 110 °C, the $|G^*|$ of the pure *t*BP-jeff$_{148}$ remained constant until polymerization reaction occurred. The final isothermal treatment was carried out at 215 °C, since a drastic reduction of the shear modulus due to thermal degradation was observed at higher temperatures (data not shown). With the addition of small amounts of GO to *t*BP-jeff$_{148}$, the initial shear modulus of the mixtures was remarkably increased, as mentioned earlier. However, during the temperature ramp, the mixtures displayed a clear temperature-dependent behavior as opposed to the *t*BP-oda series. Polymerized *t*BP-jeff$_{148}$ at 215 °C showed a larger shear modulus than *t*BP-oda polymerized at 225 °C. The aliphatic segment in the benzoxazine prepared with Jeffamine might have imparted mobility to the system during polymerization thus enhancing cross-linking density, which resulted in a higher shear modulus. In contrast with *t*BP-oda series, the nanocomposites prepared with *t*BP-jeff$_{148}$ showed no significant differences in the onset of polymerization or in the final dynamic shear modulus at 215 °C. Aggregation of the GO nanoplatelets during polymerization seemed to be one of the reasons for the lesser effect of GO in improving the shear modulus on the nanocomposites at 215 °C, as it can be seen in the picture taken after the polymerization experiments where two phases are clearly observed (picture 1, Supporting Information).

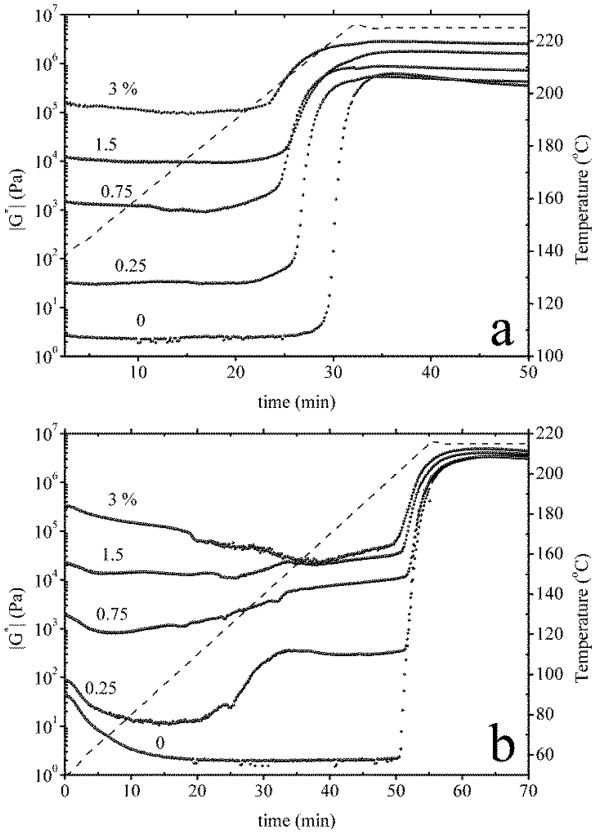

Figure 5. Dynamic shear modulus at 6.28 rad/s of (a) *t*BP-oda series and (b) *t*BP-jeff$_{148}$ series as a function of time. Dashed lines represent the temperature profile as a function of time.

The glass transition temperature T_g of the samples was obtained in a subsequent cooling experiment at 3 °C/min, 6.28 rad/s, and at 0.01% strain amplitude. Figure 6 show the storage G' and loss G'' modulus, and the tan δ of the two series as a function of the temperature. As mentioned earlier, due to poor dispersion of the GO nanosheets in poly(*t*BP-jeff$_{148}$), the mechanical properties of the thermoset above the glass transition were only slightly modified (Figure 5c). In addition, a decrease of T_g was observed with GO concentration. Figure 7 shows T_g as a function of the nanosheet filler content, determined from G'' max. The tan δ max values were also included. T_g from GO/poly(*t*BP-jeff$_{148}$) nanocomposites was reduced by 13 °C when 3 wt % GO was added. In the case of series prepared with *t*BP-oda, the dispersibility of the nanosheets was found to be better before and after polymerization, which resulted in a notable enhancement of the mechanical properties above T_g, as well as of T_g itself, as observed in Figure 6a and b. The glass transition temperature of GO/poly(*t*BP-oda) nanocomposites exhibited a shift of 15 °C to

dx.doi.org/10.1021/ma500334j | *Macromolecules* 2014, 47, 3685−3692

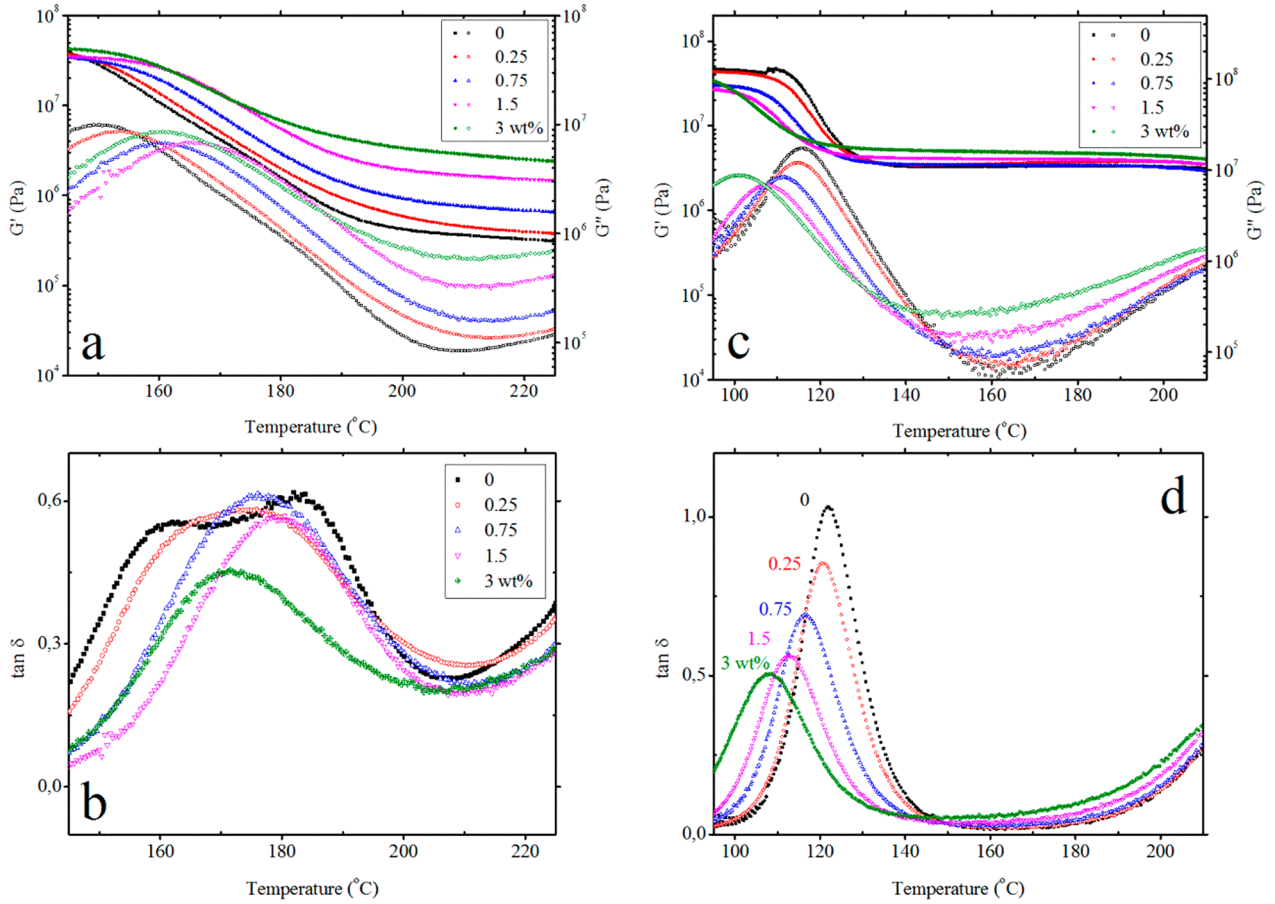

Figure 6. Storage and loss moduli, and tan δ at 6.28 rad/s and at 0.01% strain amplitude as a function of temperature for *t*BP-oda series (a and b), and for *t*BP-jeff$_{148}$ series (c and d).

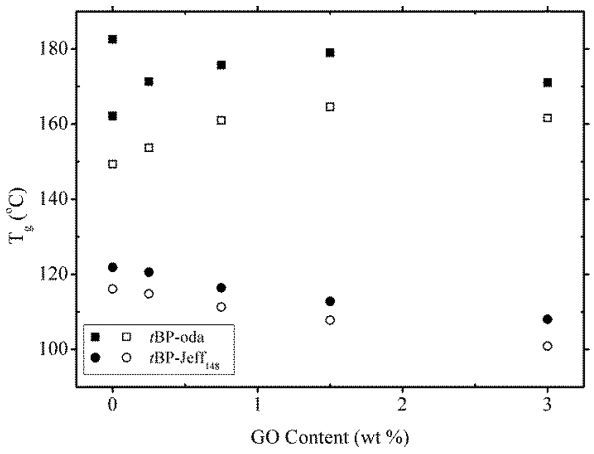

Figure 7. Glass transition temperature T_g presented by the temperature at G''_{max} (open symbols) and by tan δ_{max} (filled symbols) as a function of concentration of GO.

higher temperatures with only 1.5 wt % GO. Similar enhancements of T_g have also been observed in systems where analogous carbon fillers-based polybenzoxazine nanocomposites were studied.[51−54] Ma et al. reported an increase of 12 °C in T_g for poly(BF-ala) containing 1 wt % of covalently functionalized reduced GO with BF-ala.[51] Gu et al. also observed, from isothermal DSC experiments, an enhancement of 10 °C in T_g for poly(BA-a) nanocomposites containing 3 wt % GO.[52] Furthermore, not only a very low percolation threshold was found when multiwalled carbon nanotubes (MWNT) were added to benzoxazine monomers (BA-a and MDP-a) but also an increase of 26 °C in T_g for poly(MDP-a)/MWNT nanocomposites containing 0.1 and 0.3 wt % nanofiller.[53]

Nonetheless, two plausible factors for both enhanced dispersibility and T_g of GO/poly(*t*BP-oda) nanocomposites are then suggested in this study. One is the higher presence of aromaticity in the structure of the *t*BP-oda monomer, which would result in stronger interfacial interactions through $\pi-\pi$ stacking with the large surface of GO.[55−57] The other is the existence of hydrogen bonding between *t*BP-oda and GO. That is, upon polymerization of the oxazine ring, it has been reported that the majority of the Mannich base forms intramolecular six-membered ring with the phenolic OH group. Such a stable hydrogen bond will not participate hydrogen bonding with the GO surface. The strong amine, such as the aliphatic ether diamine used for *t*BP-Jeff$_{148}$ will lead to the intramolecular hydrogen bonding.[58] On the other hand, weak amines, such as the one used for *t*BP-oda will lead to both intra- and intermolecular hydrogen bonding.[58] Such intramolecular hydrogen bonded structure has been hypothesized to be the cause of the surface free energy of polybenzoxazines to be lower than polytetrafluoroethylene[59] and was used as the mold release agent for nanolithography.[60] It is this intermolecular hydrogen-bonded phenolic OH groups that can participate in the hydrogen bonding with the hydrophilic GO surface. Thus, the effective reinforcement effect of the polybenzoxazine derived from *t*BP-oda will lead to better reinforcement effect as observed.

dx.doi.org/10.1021/ma500334j | *Macromolecules* 2014, 47, 3685−3692

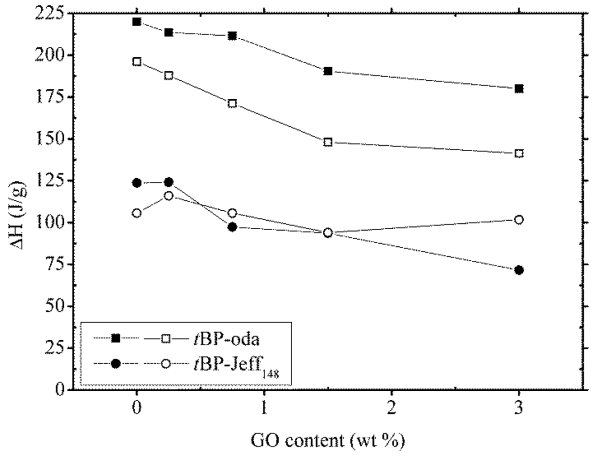

Figure 8. Enthaply of polymerization of the two series as a function of concentration of GO. Filled symbols represent the enthalpy of polymerization obtained from the standard method, and open symbols from the simulating method.

The effect of GO on the extent of polymerization of the nanocomposites was also studied. Figure 8 shows the enthalpy of polymerization of the two series as a function of concentration of GO, obtained from the standard procedure at 10 °C/min up to 300 °C, as well as by simulating the polymerization process performed in the rheometer (DSC curves are shown in Figure 5SI, Supporting Information). Increasing presence of GO nanosheets in host benzoxazines caused a continuous decrease of the heat of polymerization. With 3 wt % GO, there was a reduction in the enthalpy of polymerization of approximately 18% for the *t*BP-oda series. A more pronounced decrease was observed in the *t*BP-jeff$_{148}$ series, although its determination was overestimated due to overlapping of the deoxygenation exothermic event of GO (Figue 4SIb, Supporting Information). As expected, the heat of polymerization obtained from the simulation experiments displayed similar dependency on the GO concentration. Similar observations were obtained in a recently reported study about thermal properties of main-chain benzoxazine and GO,[61] wherein it was suggested that heat released from GO deoxygenation might have caused premature ring-opening reaction of the benzoxazine without contributing to cross-linking. It was thus suggested to be the cause for the reduction of the T_g of the cured nanocomposites. In this study, such phenomenon would have contributed to the drop in T_g for nanocomposites prepared with *t*BP-jeff$_{148}$, aggravated by GO aggregation as well. However, as it was discussed earlier, the opposite effect on T_g in GO/poly(*t*BP-oda) nanocomposites was observed. It seems therefore, that a micromechanical effect of the GO nanoplatelets (GO modulus and aspect ratio) accompanied by the degree of dispersibility had as much or even stronger influence on modifying the properties of the nanocomposites than the extent of polymerization obtained in this study.

CONCLUSION

Small amounts of graphene oxide GO (0.25 to 3 wt %) were successfully dispersed using two different reactive benzoxazine monomers as matrices, *t*BP-oda and *t*BP-jeff$_{148}$. Rheological studies of the nanocomposites showed the storage modulus G' and limit of linearity γ_c power-law dependency on the volume fraction of GO: $G' \propto \phi^{3.36}$ and $\gamma_c \propto \phi^{-0.96}$, and $G' \propto \phi^{4.33}$ and $\gamma_c \propto \phi^{-0.82}$ for *t*BP-oda and *t*BP-jeff$_{148}$ series, respectively. Quantitative analysis of the power-law scaling predictions was carried out employing the scaling model of fractal aggregates. Thus, the lower value of the fractal dimension obtained for the GO network in *t*BP-oda, $D = 2.17$ as opposed to $D = 2.43$ for the *t*BP-jeff$_{148}$ series, indicated a better dispersion of the GO nanosheets in *t*BP-oda. The polymerization behavior of the GO/Benzoxazine mixtures was also analyzed using both rheology and DSC. An increase of the dynamic shear modulus as a function of the GO content was observed for GO/poly(*t*BP-oda) nanocomposites at temperatures higher than T_g, almost one decade for samples containing 3 wt % GO. However, enhancement of the mechanical properties for the GO/poly(*t*BP-jeff$_{148}$) nanocomposites by a factor of 1.5 was observed, most likely as a consequence of reaggregation of the GO nanosheets during the polymerization process. In addition, the effect of GO on the glass transition temperature T_g was an increase for *t*BP-oda series and a decrease for *t*BP-jeff$_{148}$ series. It was found, however, that the addition of GO had a reducing effect of the extent of polymerization of both nanocomposite series, up to 20% for samples containing 3 wt % GO. Such phenomenon would explain the reduction of T_g, though only for *t*BP-jeff$_{148}$ nanocomposites. We suggest, therefore, that effective exfoliation and dispersion of GO had a greater influence on the modification of the mechanical and thermal properties of the nanocomposites. Furthermore, a stronger $\pi-\pi$ stacking interaction with nonoxidized sp^2-regions of GO of the benzoxazine monomer with higher degree of aromaticity (*t*BP-oda), as well as its ability to form intermolecular hydrogen bonding with the GO surface, may be the reason for the better dispersibility.

ASSOCIATED CONTENT

Supporting Information

X-ray diffraction patterns of graphite and graphite oxide, FT-IR spectra of *t*BP-oda and *t*BP-Jeff$_{148}$, DSC thermograms of *t*BP-oda, *t*BP-jeff$_{148}$, and GO prior to any treatment, DSC thermograms of the *t*BP-oda series and *t*BP-jeff$_{148}$ series, DSC thermograms of the *t*BP-oda series and *t*BP-jeff$_{148}$ series simulating the experiments in the rheometer, and a picture of polymerized *t*BP-jeff$_{148}$ containing 0.75 wt % GO after rheological experiments. This material is available free of charge via the Internet at http://pubs.acs.org.

AUTHOR INFORMATION

Corresponding Author

*(F.H.J.M.) E-mail: Frans.Maurer@polymat.lth.se.

Notes

The authors declare no competing financial interest.

ACKNOWLEDGMENTS

We thank the Swedish Research Council for Environment, Agricultural Sciences and Spatial Planning (Formas) for the financial support.

REFERENCES

(1) Ishida, H. In *Handbook of Benzoxazine Resins*; Ishida, H., Agag, T., Eds.; Elsevier: Amsterdam, 2011; pp 3−81.
(2) Nair, C. P. R. *Prog. Polym. Sci.* **2004**, *29* (5), 401−498.
(3) Takeichi, T.; Agag, T. *High Perform. Polym.* **2006**, *18* (5), 777−797.
(4) Ghosh, N. N.; Kiskan, B.; Yagci, Y. *Prog. Polym. Sci.* **2007**, *32* (11), 1344−1391.

(5) Sawaryn, C.; Landfester, K.; Taden, A. *Macromolecules* **2011**, *44* (19), 7668−7674.
(6) Kimura, H.; Matsumoto, A.; Sugito, H.; Hasegawa, K.; Ohtsuka, K.; Fukuda, A. *J. Appl. Polym. Sci.* **2001**, *79* (3), 555−565.
(7) Kiskan, B.; Colak, D.; Muftuoglu, A. E.; Cianga, I.; Yagci, Y. *Macromol. Rapid Commun.* **2005**, *26* (10), 819−824.
(8) Takeichi, T.; Kano, T.; Agag, T. *Polymer* **2005**, *46* (26), 12172−12180.
(9) Chernykh, A.; Liu, J.; Ishida, H. *Polymer* **2006**, *47* (22), 7664−7669.
(10) Chernykh, A.; Agag, T.; Ishida, H. *Macromolecules* **2009**, *42* (14), 5121−5127.
(11) Dogan Demir, K.; Kiskan, B.; Yagci, Y. *Macromolecules* **2011**, *44* (7), 1801−1807.
(12) Agag, T.; Arza, C. R.; Maurer, F. H. J.; Ishida, H. *J. Polym. Sci., Part A: Polym. Chem.* **2011**, *49* (20), 4335−4342.
(13) Nielsen, L. E. In *Mechanical Properties of Polymers and Composites*; Nielsen, L. E., Eds.; M. Dekker, Inc: New York, 1974; Vol. 2, p 379.
(14) Keller, T. *Prog. Struct. Eng. Mater.* **2001**, *3* (2), 132−140.
(15) Kojima, Y.; Fukumori, K.; Usuki, A.; Okada, A.; Kurauchi, T. J. *Mater. Sci. Lett.* **1993**, *12* (12), 889−890.
(16) Giannelis, E. P. *Adv. Mater.* **1996**, *8* (1), 29−35.
(17) Fornes, T. D.; Yoon, P. J.; Keskkula, H.; Paul, D. R. *Polymer* **2001**, *42* (25), 9929−9940.
(18) Ajayan, P. M.; Schadler, L. S.; Giannaris, C.; Rubio, A. *Adv. Mater.* **2000**, *12* (10), 750−753.
(19) Thostenson, E. T.; Ren, Z.; Chou, T. W. *Compos. Sci. Technol.* **2001**, *61* (13), 1899−1912.
(20) Zheng, W.; Lu, X.; Wong, S. C. *J. Appl. Polym. Sci.* **2004**, *91* (5), 2781−2788.
(21) Novoselov, K. S.; Geim, A. K.; Morozov, S. V.; Jiang, D.; Zhang, Y.; Dubonos, S. V.; Grigorieva, I. V.; Firsov, A. A. *Science* **2004**, *306* (5696), 666−669.
(22) Kotov, N. A.; Dékány, I.; Fendler, J. H. *Adv. Mater.* **1996**, *8* (8), 637−641.
(23) Kovtyukhova, N. I. *Chem. Mater.* **1999**, *11* (3), 771−778.
(24) Cassagneau, T.; Guérin, F.; Fendler, J. H. *Langmuir* **2000**, *16* (18), 7318−7324.
(25) Stankovich, S.; Dikin, D. A.; Dommett, G. H. B.; Kohlhaas, K. M.; Zimney, E. J.; Stach, E. A.; Piner, R. D.; Nguyen, S. T.; Ruoff, R. S. *Nature* **2006**, *442* (7100), 282−286.
(26) Ramanathan, T.; Abdala, A. A.; Stankovich, S.; Dikin, D. A.; Herrera-Alonso, M.; Piner, R. D.; Adamson, D. H.; Schniepp, H. C.; Chen, X.; Ruoff, R. S.; Nguyen, S. T.; Aksay, I. A.; Prud'Homme, R. K.; Brinson, L. C. *Nat. Nanotechnol.* **2008**, *3* (6), 327−331.
(27) Hummers, W. S., Jr.; Offeman, R. E. *J. Am. Chem. Soc.* **1958**, *80* (6), 1339.
(28) Brodie, B. C. *Philos. Trans. R. Soc. London* **1859**, *149*, 249−259.
(29) Staudenmaier, L. *Ber. Dtsch. Chem. Ges.* **1898**, *31*, 1481−1487.
(30) Cai, M.; Thorpe, D.; Adamson, D. H.; Schniepp, H. C. *J. Mater. Chem.* **2012**, *22* (48), 24992−25002.
(31) Parades, J. I.; Villar-Rodil, S.; Martínez-Alonso, A.; Tascón, J. M. D. *Langmuir* **2008**, *24* (19), 10560−10564.
(32) Dreyer, D. R.; Park, S.; Bielawski, C. W.; Ruoff, R. S. *Chem. Soc. Rev.* **2010**, *39* (1), 228−240.
(33) Suk, J. W.; Piner, R. D.; An, J.; Ruoff, R. S. *ACS Nano* **2010**, *4* (11), 6557−6564.
(34) Lin, E. K.; Wu, W. L.; Satija, S. K. *Macromolecules* **1997**, *30* (23), 7224−7231.
(35) Starr, F. W.; Schrøder, T. B.; Glotzer, S. C. *Macromolecules* **2002**, *35* (11), 4481−4492.
(36) Bansal, A.; Yang, H.; Li, C.; Cho, K.; Benicewicz, B. C.; Kumar, S. K.; Schadler, L. S. *Nat. Mater.* **2005**, *4* (9), 693−698.
(37) Desai, T.; Keblinski, P.; Kumar, S. K. *J. Chem. Phys.* **2005**, *122* (13), 134910.
(38) Harmandaris, V. A.; Daoulas, K. C.; Mavrantzas, V. G. *Macromolecules* **2005**, *38* (13), 5796−5809.
(39) Ramanathan, T.; Liu, H.; Brinson, L. C. *J. Polym. Sci., Part B: Polym. Phys.* **2005**, *43* (17), 2269−2279.
(40) Vermant, J.; Ceccia, S.; Dolgovskij, M. K.; Maffettone, P. L.; Macosko, C. W. *J. Rheol.* **2007**, *51* (3), 429−450.
(41) Marcano, D. C.; Kosynkin, D. V.; Berlin, J. M.; Sinitskii, A.; Sun, Z.; Slesarev, A.; Alemany, L. B.; Lu, W.; Tour, J. M. *ACS Nano* **2010**, *4* (8), 4806−4814.
(42) Buscall, R.; Mills, P. D. A.; Stewart, R. F.; Sutton, D.; White, L. R.; Yates, G. E. *J. Non-Newtonian Fluid Mech.* **1987**, *24* (2), 183−202.
(43) Buscall, R.; Mills, P. D. A.; Goodwin, J. W.; Lawson, D. W. *J. Chem. Soc., Faraday Trans. 1* **1988**, *84* (12), 4249−4260.
(44) Martin, J. E.; Wilcoxon, J.; Adolf, D. *Phys. Rev. A: At., Mol., Opt. Phys.* **1987**, *36* (4), 1803−1810.
(45) Shih, W. H.; Shih, W. Y.; Kim, S. I.; Liu, J.; Aksay, I. A. *Phys. Rev. A: At., Mol., Opt. Phys.* **1990**, *42* (8), 4772−4779.
(46) Gazzano, M.; Tomasi, G.; Scandola, M. *Macromol. Chem. Phys.* **1997**, *198* (1), 71−80.
(47) Ren, J.; Silva, A. S.; Krishnamoorti, R. *Macromolecules* **2000**, *33* (10), 3739−3746.
(48) Stankovich, S.; Dikin, D. A.; Dommett, G. H. B.; Kohlhaas, K. M.; Zimney, E. J.; Stach, E. A.; Piner, R. D.; Nguyen, S. T.; Ruoff, R. S. *Nature* **2006**, *442* (7100), 282−286.
(49) Kim, H.; Macosko, C. W. *Macromolecules* **2008**, *41* (9), 3317−3327.
(50) Liu, N.; Luo, F.; Wu, H.; Liu, Y.; Zhang, C.; Chen, J. *Adv. Funct. Mater.* **2008**, *18* (10), 1518−1525.
(51) Ho, K.-K.; Hsiao, M.-C.; Chou, T.-Y.; Ma, C.-C. M.; Xie, X.-F.; Chiang, J.-C.; Yang, S.-h.; Chang, L.-H. *Polym. Int.* **2013**, *62* (6), 966−973.
(52) Zeng, M.; Wang, J.; Li, R.; Liu, J.; Chen, W.; Xu, Q.; Gu, Y. *Polymer* **2013**, *54* (12), 3107−3116.
(53) Zuniga, C.; Bonnaud, L.; Lligadas, G.; Ronda, J. C.; Galia, M.; Cadiz, V.; Dubois, P. *J. Mater. Chem. A* **2014**, *2* (19), 6814−6822.
(54) Chen, Q.; Xu, R.; Yu, D. *Polymer* **2006**, *47* (22), 7711−7719.
(55) Chen, Z.; Lohr, A.; Saha-Möller, C. R.; Würthner, F. *Chem. Soc. Rev.* **2009**, *38* (2), 564−584.
(56) Lu, C. H.; Yang, H. H.; Zhu, C. L.; Chen, X.; Chen, G. N. *Angew. Chem., Int. Ed.* **2009**, *48* (26), 4785−4787.
(57) Yang, X.; Zhang, X.; Liu, Z.; Ma, Y.; Huang, Y.; Chen, Y. J. *Phys. Chem. C* **2008**, *112* (45), 17554−17558.
(58) Kim, H. D.; Ishida, H. *J. Phys. Chem. A* **2002**, *106* (14), 3271−3280.
(59) Wang, C. F.; Su, Y. C.; Kuo, S. W.; Huang, C. F.; Sheen, Y. C.; Chang, F. C. *Angew. Chem., Int. Ed.* **2006**, *45* (14), 2248−2251.
(60) Wang, C. F.; Chiou, S. F.; Ko, F. H.; Chen, J. K.; Chou, C. T.; Huang, C. F.; Kuo, S. W.; Chang, F. C. *Langmuir* **2007**, *23* (11), 5868−5871.
(61) Alhassan, S. M.; Qutubuddin, S.; Schiraldi, D. A.; Agag, T.; Ishida, H. *Eur. Polym. J.* **2013**, *49* (12), 3825−3833.